Journal of Materials Chemistry C

ROYAL SOCIETY OF CHEMISTRY

PAPER

View Article Online
View Journal | View Issue

Cite this: J. Mater. Chem. C, 2023, 11, 13752

Self-healing electrochromic energy storage devices based on PEDOT:PSS†

Yuanze Meng,[a] Jialun Li,[a] Xijia Yang,[a] Yang Gao,[a] Xuesong Li,[a] Liying Wang *[a] and Wei Lü *[ab]

Received 13th July 2023,
Accepted 6th September 2023

DOI: 10.1039/d3tc02458j

rsc.li/materials-c

Poly (3,4-ethylenedioxythiophene): poly (4-styrenesulfonic acid) (PEDOT:PSS) is a kind of widely used polymer with excellent electrical conductivity. In this study, PEDOT:PSS was modified to achieve self-healing ability while maintaining excellent energy storage properties. The modified PEDOT:PSS hybrid film demonstrated instantaneous self-healing ability due to physical cross-linking after being subjected to different external cuts (the average self-healing time was 1.44 s). When pressed at different rates, the film had a self-healing time of less than 0.12 s, and a retention rate of 74% after pressing 1750 times consecutively at a rate of 8.6 cm s^{-1}. The mechanism of self-healing was investigated using theoretical calculations. Tungsten trioxide (WO_3) was further introduced into the PEDOT:PSS hybrid film to fabricate electrochromic energy storage devices (EESDs), achieving a specific capacitance of 105.35 mF cm^{-2} and a capacitance retention of 98.2% after 1000 cycles. In the organic/inorganic hybrid system, the modified PEDOT:PSS film acted as both a protective coating for WO_3 and exhibited a synergistic color change with WO_3, ultimately improving the overall performance of the device. The present self-healing strategy can help design restorers for EESDs and can be extended to other new rechargeable electrochromic battery systems with good application prospects.

1. Introduction

Cracking, breakage, and failure have long been challenging issues affecting the application of materials. Inspired by the self-healing behavior of living organisms in nature, researchers have introduced the concept of self-healing in materials. This innovation allows materials to be repaired under specific conditions, thereby extending their service life and preventing overuse and waste of resources.[1–4] As a result, self-healing materials have attracted significant attention in various fields, including protective coatings, visual devices and sensors, *etc.* Du *et al.* synthesized polyurethane/graphene repair coating materials containing diselenide bonds by incorporating graphene oxide into polyurethane, which maintained self-healing efficiency of over 75% after 5 healing cycles.[5] Deng *et al.* introduced triphenylamine (TPA) into the polymerization reaction and synthesized a non-conjugated TPA-based polymer DATPFMA, which had multiple color variations and demonstrated self-healing ability at 110 °C.[6] Zheng *et al.* added TPA and self-healing Diels–Alder groups to create a high-performing polymer called PPFMA with effective cycling stability improvement.[7] A polyvinyl alcohol-borax-ionic liquid composite gel prepared by Liu *et al.* exhibited good repairability and bending sensitivity.[8]

In recent years, self-healing has emerged as a popular research topic in the field of energy storage systems. Numerous related studies have been reported. Zhao *et al* prepared a lithium-ion battery loaded with $LiMn_2O_4$ and $LiTi_2(PO_4)_3$ nanoparticles on a self-healing polymer.[9] This battery underwent five cycles of cutting/healing, and its performance was effectively maintained. Long *et al.* introduced a self-healing electrolyte and synthesized a zinc ion supercapacitor, which exhibited stable capacity even after undergoing damage and subsequent healing.[10] However, most self-healing energy storage devices are fabricated with a primary focus on the repairability of gel electrolytes. Studies involving restorative electrodes also require loading conductive materials to enhance conductivity and energy storage performance, which undoubtedly complicates the preparation process. Therefore, it is highly necessary to investigate self-healing electrode materials that exhibit good energy storage performance.

PEDOT:PSS is a conductive polymer that is widely used in various applications such as supercapacitors,[11,12] solar cells,[13]

[a] Key Laboratory of Advanced Structural Materials, Ministry of Education, School of Materials Science and Engineering, and Advanced Institute of Materials Science, Changchun University of Technology, Changchun, 130012, China. E-mail: wangliying@ccut.edu.cn, lw771119@hotmail.com; Fax: +86-0431-85716577; Tel: +86-0431-85716577

[b] State Key Laboratory of Luminescence and Applications, Changchun Institute of Optics, Fine Mechanics and Physics, Chinese Academy of Sciences, Changchun 130033, China

† Electronic supplementary information (ESI) available. See DOI: https://doi.org/10.1039/d3tc02458j

and light-emitting diodes,[14] owing to its excellent electrical properties, optical properties, and sensitivity to mechanical strain. Furthermore, PEDOT:PSS also shows self-healing capabilities. Li *et al.* have confirmed that the PEDOT:PSS film can self-repair when exposed to water after being cut, but the self-healing function disappears upon drying.[15] Therefore, in order to achieve self-healing properties without external intervention, a blend of other polymers is necessary. Self-healing PEDOT:PSS films can be prepared by adding surfactant Triton X-100[16,17] or polyethylene glycol (PEG).[18] However, Triton X-100 is potentially hazardous, making it unsuitable for widespread application.

Based on the aforementioned discussion, developing energy storage devices with self-healing function based on PEDOT:PSS could be a promising way to fabricate energy storage devices with great application potential. In the present work, we prepared hybrid organic films by modifying PEDOT:PSS with PEG and phytic acid (PA) to achieve both energy storage and instantaneous self-healing capabilities. Modified PEDOT:PSS organic mixtures could achieve self-healing ability due to physical cross-linking resulting from hydrogen bonding. And, we further explained the self-healing mechanism of the organic mixture from the perspective of electrostatic potential using simulations. Organic polymers alone, however, do not exhibit the same level of chemical stability as inorganic transition metal oxides. Conversely, capacitance and energy density of organic/inorganic hybrid systems can be increased, while also improving other properties by their interfacial interactions.[19,20] For example, Ling *et al.* have demonstrated the preparation of PEDOT:PSS/WO_3 hybrid films with good cycling stability using electrodeposition.[21]So, we fabricated composite electrode films by employing modified PEDOT:PSS as a protective coating and combining it with WO_3, as depicted in Fig. 1.

The composite of PEDOT:PSS and WO_3 is not only employed as an energy storage material, but also as a cathodic electrochromic material exhibiting synergistic color-changing behavior under the influence of negative voltage.[22] Incorporating organic hybrid films effectively enhances the overall performance of a device. This self-healing approach can provide insight into designing repair agents for electrochemical energy storage systems and could be extended to other emerging rechargeable electrochromic battery systems.

2. Experimental section

2.1. Chemicals

FTO glass was purchased from Zhuhai Kevo Photoelectric Technology Co., Ltd. Hydrochloric acid, acetone, ethanol, isopropanol and polyethylene glycol were purchased from Tianjin Fuyu Fine Chemical Co., Ltd. Sodium tungstate (Na_2WO_4), citric acid (CA), ammonium chloride (NH_4Cl), polyethyleneimine (PEI), phytic acid (PA), and poly (3,4-ethylenedioxythiophene): poly (4-styrenesulfonic acid) (PEDOT:PSS) were purchased from Shanghai Aladdin Biochemical Technology Co., Ltd. All chemicals were used directly without further purification.

2.2. Preparation of the WO_3-PEI film

FTO glass (2.5 cm × 1.5 cm) was ultrasonically cleaned with deionized water, acetone, isopropanol, ethanol and deionized water for 15 min. 0.5 g Na_2WO_4 powder, 0.3 g CA powder and 0.35 g NH_4Cl powder were added to 30 mL deionized water and stirred until they dissolved. 3 mol L^{-1} hydrochloric acid solution was further added to the mixed solution until the solution pH becomes 0.5 under stirring. The FTO conductive

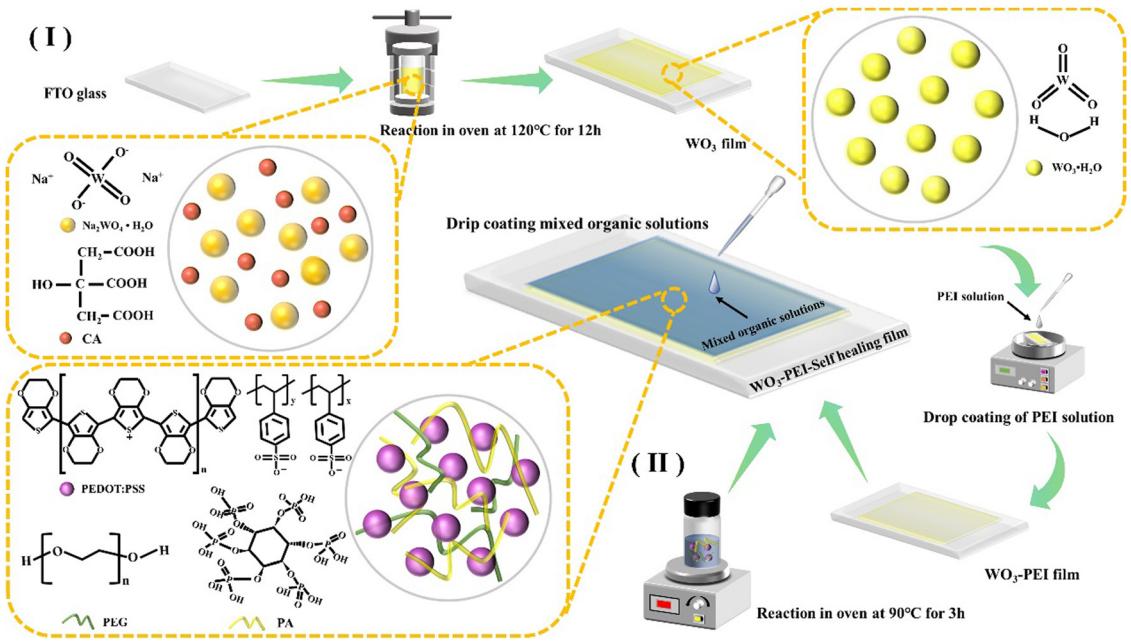

Fig. 1 Preparation process diagram and related mechanism diagram of the WO_3-PEI-self healing film. (I) Preparation process of the WO_3-PEI film. (II) Preparation process of mixed organic solutions.

glass surface was put into the solution, and placed in an oven at 120 °C for 12 h. After the reaction, the conductive glass grown with WO_3 was washed with deionized water and dried in an oven at 60 °C.

An appropriate amount of PEI was used to prepare a solution with a mass fraction of 0.4 wt%. The solution was spin-coated on the WO_3 film at a speed of 3000 rpm min^{-1} for 40 s using a spin coating machine. The WO_3 film coated with PEI was dried in an oven at 60 °C. Spin-coated PEI was used to improve the bonding effect of the WO_3 film mixed with the organic film.

2.3. Preparation of the WO_3-PEI-Self-healing film

To prepare a mixed organic solution, 3 mL of PEDOT:PSS solution was taken, to which 4% PEG solution was added and then stirred well, followed by the addition of 4.5% PA solution. The mixed solution was placed in an oven at 90 °C for 3 h. Then the mixed solution was dropped on the prepared WO_3-PEI film, and the film was dried in an oven at 60 °C for 12 h. The preparation of a PEI-Self-healing film is explained in the ESI.†

2.4. Assembling electrochromic self-healing energy storage devices

A glass fiber (GF/D) separator was placed between two thin film electrodes, and the size of the separator was 1 cm × 1 cm. Sulfuric acid solution was added to the septum and the two film electrodes are fixed with dovetail clips.

2.5. Characterization

The surface morphology and the structure of materials were analyzed by scanning electron microscopy (Hitachi Regulus8100), transmission electron microscopy (Co., Ltd), X-ray diffractometry (Bruker D8 advance), Fourier transform infrared spectroscopy (IRTracer-100, SHIMADZU), and Raman spectrometry (Renishaw 2000). The absorption and transmission spectra were recorded using an ultraviolet-visible-near-infrared spectrophotometer (Agilent CARY 5000). The film was repeatedly pressed with a uniform circulating reciprocating motor to test its self-healing performance.

2.6. Electrochemical measurements

Electrochemical tests of self-healing electrochromic energy storage devices were performed on an electrochemical workstation (CHI660E, Shanghai, China). Detailed experimental details are described in the ESI.† In the following discussion, the WO_3-PEI film was defined as the WP film, the PEI-Self healing film was defined as the PSH film, and the WO_3-PEI-Self healing film was defined as the WPSH film.

3. Results and discussion

The morphologies of WPSH and other films were characterized using SEM, TEM and XRD. In the low magnification SEM image of the WP film (Fig. S1a, ESI†), the surface of the FTO conductive glass is uniformly and tightly covered by a large number of nanosheet structures. In the high magnification SEM image (Fig. S1b, ESI†), the sheet thickness is uniform and the surface is smooth. These nanosheets are in close contact with each other. The two-dimensional nanosheets can significantly increase the surface area and shorten the diffusion distance of H^+ ions, which is conducive to their insertion and extraction, and can accelerate the charge transport during the redox process. In Fig. S1c and Fig. 2a (ESI†), the adjacent nanosheet structures are filled with the prepared organic mixture, and the nanosheet is also covered with the organic mixture. Previous studies have shown that partial removal of PSS by phytate induction resulted in the conformational change of PEDOT from the benzylic to quinine structure and enhanced π–π stacking between PEDOT chains.[23] At the same time, the ionic interaction between PEDOT and PSS is shielded by the hydrogen bond between polyethylene glycol and PSS, resulting in the phase separation of the two, which is conducive to the formation of an aggregated PEDOT structure. These two reasons combinedly contributed to the physical crosslinking.[15] The mixed organic film formed a porous network structure, which further increased the area of the reaction and was also beneficial to the movement and reaction of H^+ ions. In the EDS energy spectrum of Fig. 2b, W, O, N, P and S elements are evenly distributed, indicating that WO_3, PEI and the organic mixture coexist. Fig. 2c and d show the TEM images of the PSH film and WP film. The former shows that the organic mixture has a loose structure and many pores, which is conducive to the diffusion and distribution of the electrolyte. The distribution of WO_3 nanosheets can be clearly observed in the latter. Fig. 2e indicates that W, O and N elements are present and evenly distributed, which reflects that we have successfully prepared the WP films. Fig. 2f shows the TEM images of the WPSH film. WO_3 is wrapped by the organic mixture. Fig. S1h (ESI†) indicates that a stripe spacing of 0.37 nm corresponds to the (120) crystal plane of WO_3, which proves the existence of WO_3. In Fig. 2h, the elements of W, O, N, P and S are evenly distributed. At the same time, the energy spectrum in Fig. 2i shows that the film contains the above elements, which indicates the successful preparation of the WPSH film. The XRD pattern of the WP film shown in Fig. 2j was found to match with that of the orthogonal phase $WO_3{\cdot}H_2O$ shown in the standard card (JCPDS No. 43-0679).[24] The diffraction peak is sharp and the intensity is high, indicating that the crystallinity of the sample is high. Fig. 2k shows that WO_3 contained in the WPSH composite is also in an orthogonal phase (JCPDS No. 43-0679). At the same time, because the mixed organic material does not have good crystallinity, it has no obvious diffraction peak, which can also be seen in Fig. S2b (ESI†). Compared with the WP film, the composite structure of the WPSH film can provide a large number of catalytic active sites and good conductivity, thus promoting the conversion of the electrolyte.

In the FTIR spectrum of the WP film (Fig. S4a, ESI†), infrared peaks can be observed near 3424 cm^{-1} and 1635 cm^{-1}, which correspond to the vibration mode of water molecules. There is a phase transition near 935 cm^{-1}, which is weak and can be attributed to the W═O group or the terminal W–O group in

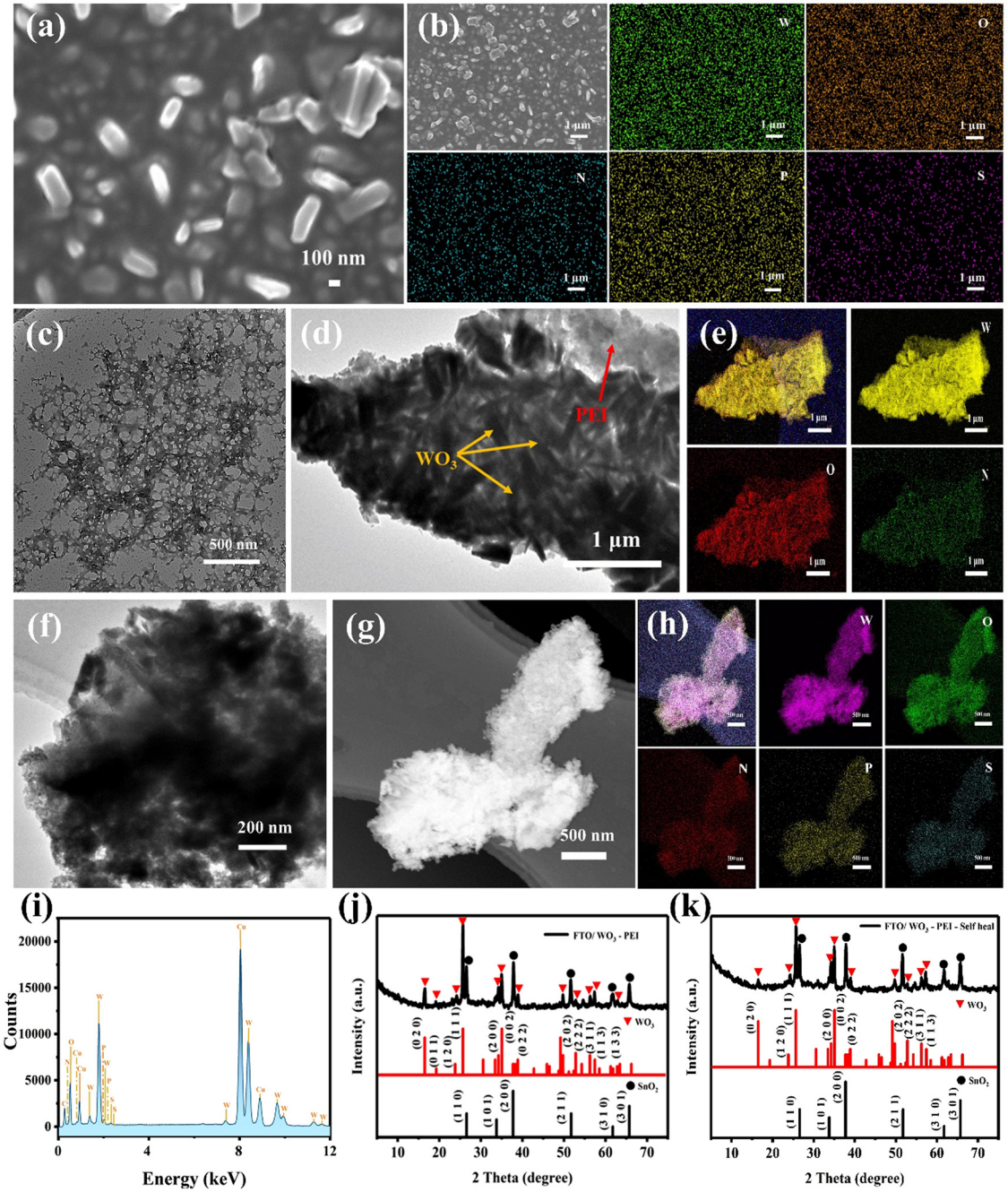

Fig. 2 (a) SEM image and (b) EDS mappings images of the WPSH film. (c) TEM image of the PSH film. (d) TEM image and (e) EDS mappings images of the WP film. (f) TEM image, (g) TEM image in the dark field, (h) EDS mappings images, (i) EDS spectra of the WPSH film. XRD patterns of (j) the WP film and (k) the WPSH film.

the amorphous compound. There is another phase transition near 731 cm^{-1}, which is attributed to the W–O stretching mode.[25–27] For the PSH film in Fig. S4b (ESI†), the 1712 cm^{-1} (C–O–H bending) peak and the 3398 cm^{-1} (O–H stretching band of hydroxyl group) peak indicate that the hydroxyl group of polyethylene glycol formed a hydrogen bond with the sulfonic group of PEDOT:PSS. The peak near 2927 cm^{-1} corresponds to the stretching vibration of the C–H bond on the PSS chain. The C–S bond vibration peak of the thiophene ring occurs near 831–690 cm^{-1}. The peak at 1197–1080 cm^{-1} is related to the S–O asymmetric vibration of the sulfonate group on the PSS chain.[28–30] In the spectrum of the WPSH film (Fig. S4c, ESI†), we can observe the related peaks of $WO_3 \cdot H_2O$ and PEDOT:PSS, which proves the successful preparation of the film. In the Raman spectrogram of the WPSH film (Fig. S5, ESI†), the peaks of $WO_3 \cdot H_2O$ are complex, mainly located near 430, 575, 706, 885 and 995 cm^{-1}.[31] The Raman peak near 706 cm^{-1} corresponds to the O–W–O asymmetric stretching vibration, and the Raman

peak near 995 cm^{-1} is attributed to the vibration mode of the terminal W=O group.[32,33] The asymmetric vibration peak of the C_α=C_β double bond in PEDOT:PSS shifts from 1521 cm^{-1} to 1536 cm^{-1}, and the peak at 1437 cm^{-1} can be considered as due to the symmetric vibration of the C_α=C_β double bond on the five-membered ring of PEDOT, while the vibration peak of the C–C single bond stretching deformation in PEDOT:PSS shifts from 1375 to 1360 cm^{-1}.[34,35] The shift of the vibration peak indicates that there is a hydrogen bond interaction between PEG, PA and PEDOT:PSS during film preparation.[36] The results of Raman diffraction are consistent with the results of SEM, TEM scanning and infrared spectroscopy.

The theoretical analysis of the coordination formation of the organic mixture was further carried out using energy calculations. A computational model was constructed based on the structure consisting of PEDOT:PSS, PEG and PA. Fig. 3a shows the preparation process of the organic mixture. Fig. 3b shows the constructed model. According to the calculations, the energy $E_{(Mix)}$ of the organic mixture is −275 742.9 eV. While the energy $E_{(PEG)}$ of PEG, energy $E_{(PA)}$ of PA and energy $E_{(PP)}$ of PEDOT:PSS are −7218.207 eV, −110 224.26 eV and −158 269.68 eV, respectively. The energy difference ΔE of the system before and after the mixing reaction is calculated using the followed equation:

$$\Delta E = E_{(Mix)} - \left(E_{(PEG)} + E_{(PA)} + E_{(PP)}\right) \quad (1)$$

ΔE = −30.753 eV. It is shown that the energy of the mixed system is less than the sum of the energy of the system without

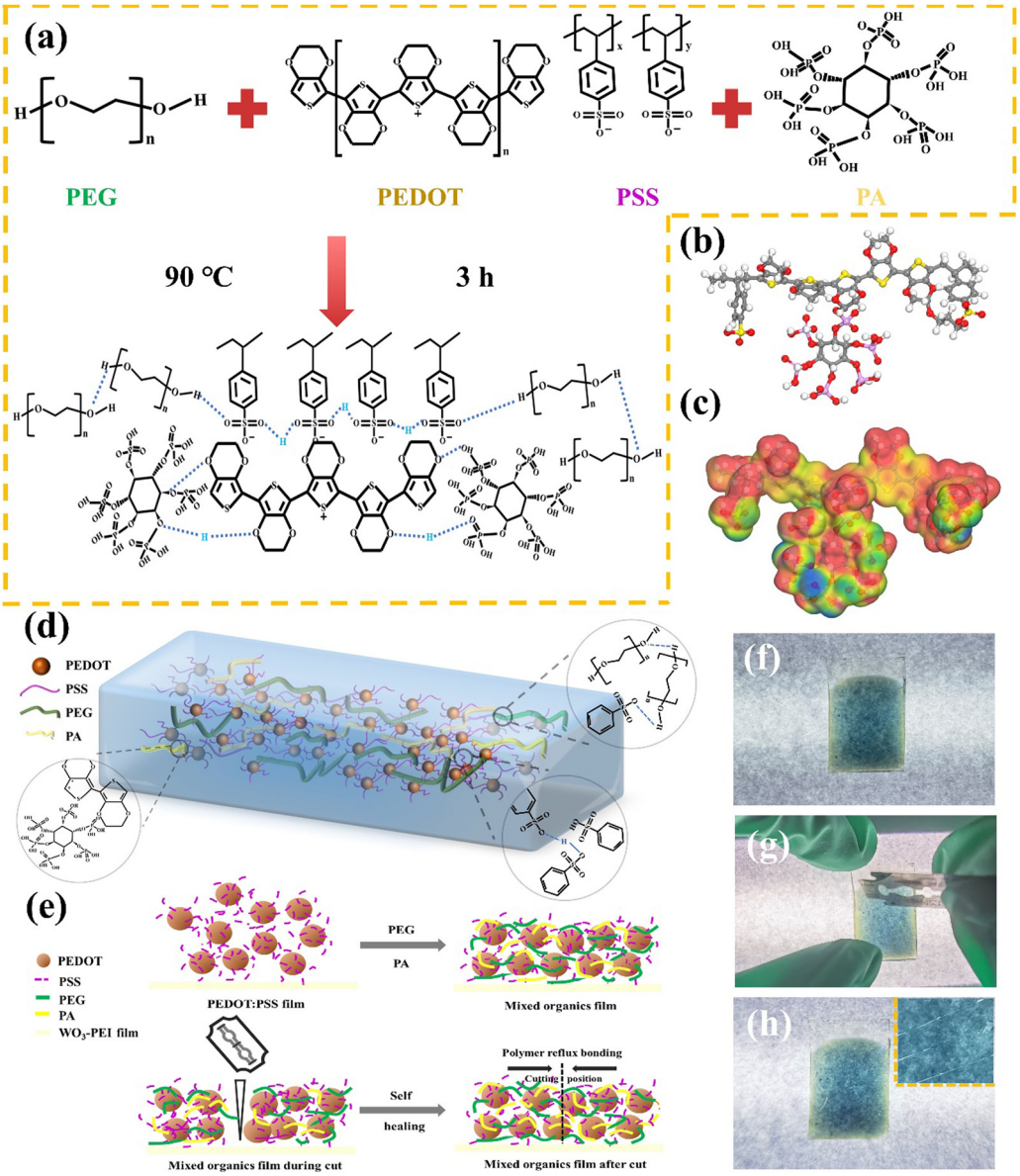

Fig. 3 (a) Preparation of the organic mixture. (b) Energy calculation model for the organic mixture. (c) Electrostatic potential of the organic mixture. (d) Microscopic diagram of the mixed organic film. (e) Diagram of the cutting and self-healing process of the mixed organic film. (f)–(h) Digital photographs of film cutting and self-healing.

mixing, which indicates that cross-linking occurs between the three organics.[37] Thus, the successful preparation of the hybrid organic films was demonstrated.

Because only the mixed organic film has self-healing properties, the self-healing experiment is only carried out for the mixed organic film. Fig. 3c shows the electrostatic potential diagram of the organic mixture. Fig. 3d shows a schematic diagram of the mixed organic film. In the presence of PEG and PA, the separation degree of PEDOT and PSS increases, which makes PEDOT aggregate and improves the conductivity of the film.[15,23] Previous studies have demonstrated that the addition of PEG can change the mechanical properties of PEDOT:PSS, enhancing the viscoelastic properties and elongation at break.[18] And the addition of PA can enhance the physical cross-linking of PEDOT and promote the generation of hydrogen bonds,[22,23] which allow the modified PEDOT:PSS films to be reconnected by automatic physical cross-linking when a gap is created. At the same time, as shown in Fig. 3e, the PEG chains also act as soft substrates for PEDOT:PSS, allowing good entanglement and mixing between the hydrophilic PSS chains, and the phosphate groups in PA, which have strong chelating effects, can also interact with the PEDOT chains. The formation of PSS-PSS, PEG-PEG, PEG-PSS, and PEDOT-PA chains between hydrogen bonds facilitates the repair process, which in turn equally facilitates the flow of materials back to the damaged area after cutting.

From another point of view, the self-healing process of thin films can be explained by the influence of electrostatic potential. The electrostatic potential is caused by the charge distribution inside the film and the presence of an electric field in the film.[38] When damage occurs in the film, the imbalance of charges leads to a change in the electrostatic potential. Around the damaged area, a region of higher electrostatic potential may be formed due to the imbalance in charge distribution caused by the damage.[38] This higher electrostatic potential can generate a stronger electric field, which facilitates the attraction of the film toward the damaged area and re-crosslinking. In Fig. 3c, The red part of the graph indicates a strong electrostatic potential, and the blue color indicates a weak electrostatic potential. The red part also happens to be the location where hydrogen bonding exists, which proves that the mixed organic film can self-heal through hydrogen bonding. Fig. 3f–h are digital photographs of the film before and after self-healing. It can be seen that the film can achieve self-healing after making scratches with blade cutting (Video S1 in the ESI† also proves that). However, the film did not self-heal when the scratch is larger than 20 μm (Fig. S7, ESI†).

The self-healing of mixed organic films under different scenarios, such as cutting and pressing, was simulated.

The film was cut multiple times with a stainless steel blade (Fig. 4a). And each cut makes a gap in the film, and the current would decrease briefly. However, due to the self-healing of the film (the average time of film self-healing is 1.43 s), the current would increase rapidly and return to normal. The stainless steel blade is electrically conductive, which can have some effect on the cutting experiments, in order to exclude the effect and more

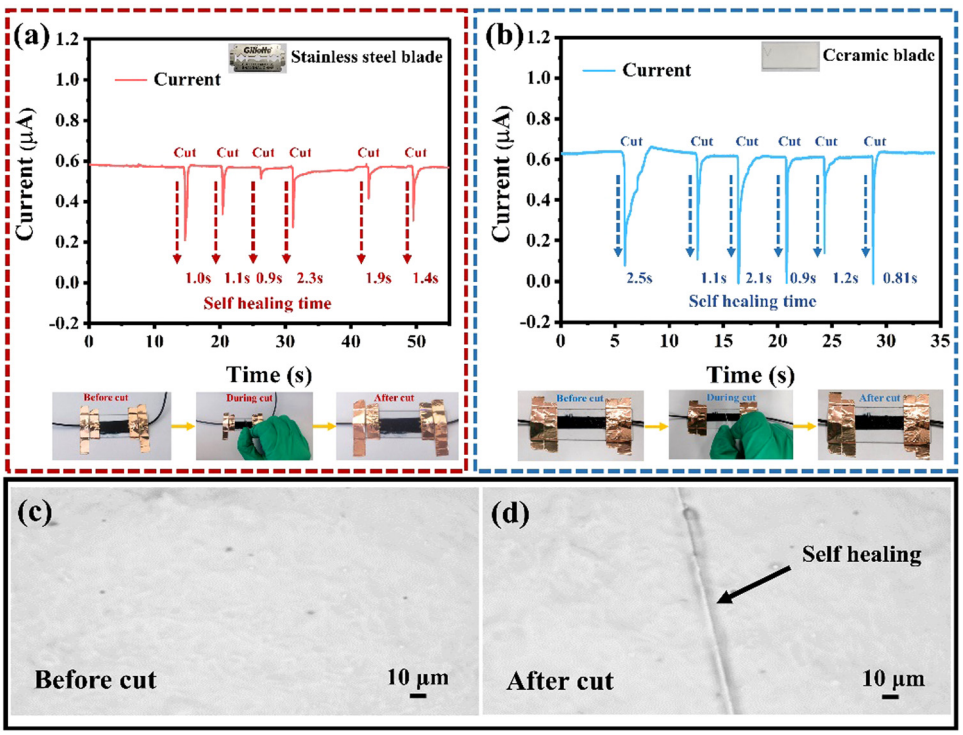

Fig. 4 (a) The current change diagram of a stainless steel blade during the cyclic cutting/self-healing process. (b) The current change diagram of a ceramic blade during the cyclic cutting/self-healing process. The illustrations from left to right are the film state before cutting, during cutting and after cutting. 100× optical microscope image of (c) the film surface and (d) self-healing after cutting.

fully demonstrate the self-healing properties of the film, under the same conditions, the film was cut by a ceramic blade (Fig. 4b), and the current could still be quickly recovered (the average time of film self-healing is 1.44 s), which showed that the film has good self-healing performance. Fig. 4c and d show the surface of the mixed organic film 100 times larger under the optical microscope and the morphology after cutting. It can be seen that after the film has been cut, the organic mixture on both sides is physically cross-linked and reflowed together to achieve self-healing.

As shown in Fig. S8 (ESI†), the film in the circuit is capable of lighting a bulb, indicating the conductivity of the film. Stainless steel blades (Video S2, ESI†) and ceramic blades (Video S3, ESI†) were used for multiple cutting. It could be seen that the bulb is not extinguished due to the cutting of the film, which also proved that the film's self-healing time was extremely short and the self-healing performance was excellent.

As shown in Fig. 5a, we used a uniform circulating reciprocating motor to simulate the pressing scene and test the self-healing performance of the film. In Fig. 5b, different gears were used to continuously press the film. Under different speeds of pressing, the self-healing time of the film was very short, reflecting its excellent performance. The film was continuously pressed for 1750 times by adjusting the gear of the motor to nine gears (8.6 cm s^{-1}). In the early stage of pressing, the film deformed greatly, making the overall current decrease more obvious. After 400 s, the film reached the deformation balance and the change of current tended to be stable. At the end of the pressing, the current drop was not large. The film had a retention rate of 74% relative to the state of deformation equilibrium, and a retention rate of 57% relative to the state at the beginning of pressing (Fig. 5c). In Fig. S10 (ESI†), we performed another 1660 nine-step cyclic pressing experiments on the film after a period of pressing. After the pressing, it still has a retention rate of 58%, indicating its good self-healing ability. Interestingly, we dropped and dried the mixed organic film on the non-conductive plastic sheet, and also carried out the pressing experiment (Fig. S9, ESI†), and the film still showed good self-healing performance. The film was pressed 1750 times, and the film had a retention rate of 82.5% compared to the state of deformation equilibrium. Compared with the state at the beginning of pressing, there was a 65.2% retention rate. At the ninth gear, 1660 cycles of pressing were also performed on the film after a period of pressing, and the

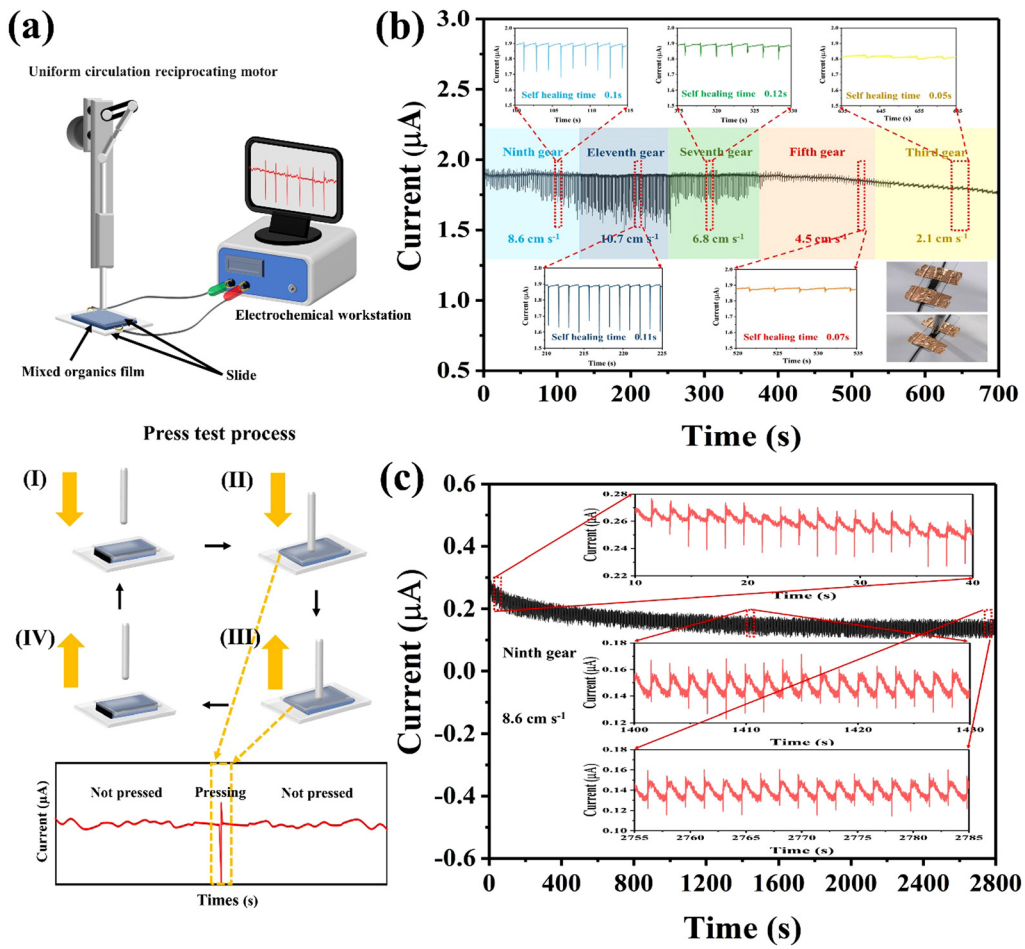

Fig. 5 (a) Schematic diagram of the pressing experiment. The film drop-coated on the slide was subjected to (b) compression experiments at different gears and (c) cyclic compression experiments at nine gears.

retention rate was still 57.5%. The excellent self-healing properties of the mixed organic film indicate that it has good application prospects in flexible energy storage devices.

The electrochemical properties of electrochromic self-healing energy storage devices are shown in Fig. 6i. Fig. 6d and e show the CV curve and GCD curve of the WPSH device, respectively. In the CV curve of the WPSH device, the square root of different scanning rates and the peak current density were fitted, and the results are shown in Fig. S12 (ESI†). This approximate linear relationship indicates that the embedding/deembedding of H^+ in the electrode is a diffusion-controlled process and also indicates the good reversibility of the redox reaction of H^+ in the film. Fig. 6f shows the electrochemical impedance spectroscopy (EIS) curve of the WPSH device. At a current density of 0.1 mA cm^{-2}, a surface capacitance of 105.35 mF cm^{-2} was obtained, which was much larger than the surface capacitance of 38 mF cm^{-2} obtained for the WP device at the same current density. By comparing the two devices (Fig. S13a, ESI†), it can be seen that the semi-circular radius of the WPSH device in the high frequency region is small, and the slope of the straight line in the low frequency region is large, which confirms that it has a low charge transfer resistance. The related electrochemical properties of the PSH device are shown in Fig. S11 (ESI†).

Fig. 6g and h show the capacitance retention of the WP device and WPSH device. Interestingly, in the WP device, the retention rate began to decrease from the beginning to the 500th cycle, but began to increase after that. The reasons are as follows: first, the discharge time will affect the change of the capacity retention rate because the current density is small and H^+ mainly depends on the concentration gradient in the electrolyte movement.[39,40] In the first 500 cycles, the concentration of H^+ gradually decreased, the rate of H^+ removal from the lattice of WO_3 was accelerated by the concentration gradient force, the discharge time was shortened, and the retention rate began to decrease. However, after the 500th cycle, the concentration of H^+ in the electrolyte increases to a certain extent, and the concentration gradient force greatly increases the difficulty of H^+ removal from WO_3, and the discharge kinetics is weakened, thereby prolonging the discharge time and improving the retention rate.

Secondly, during the cycle, the material becomes more suitable for the interface environment, and the electrolyte and the material come into more full contact.[41] In other words,

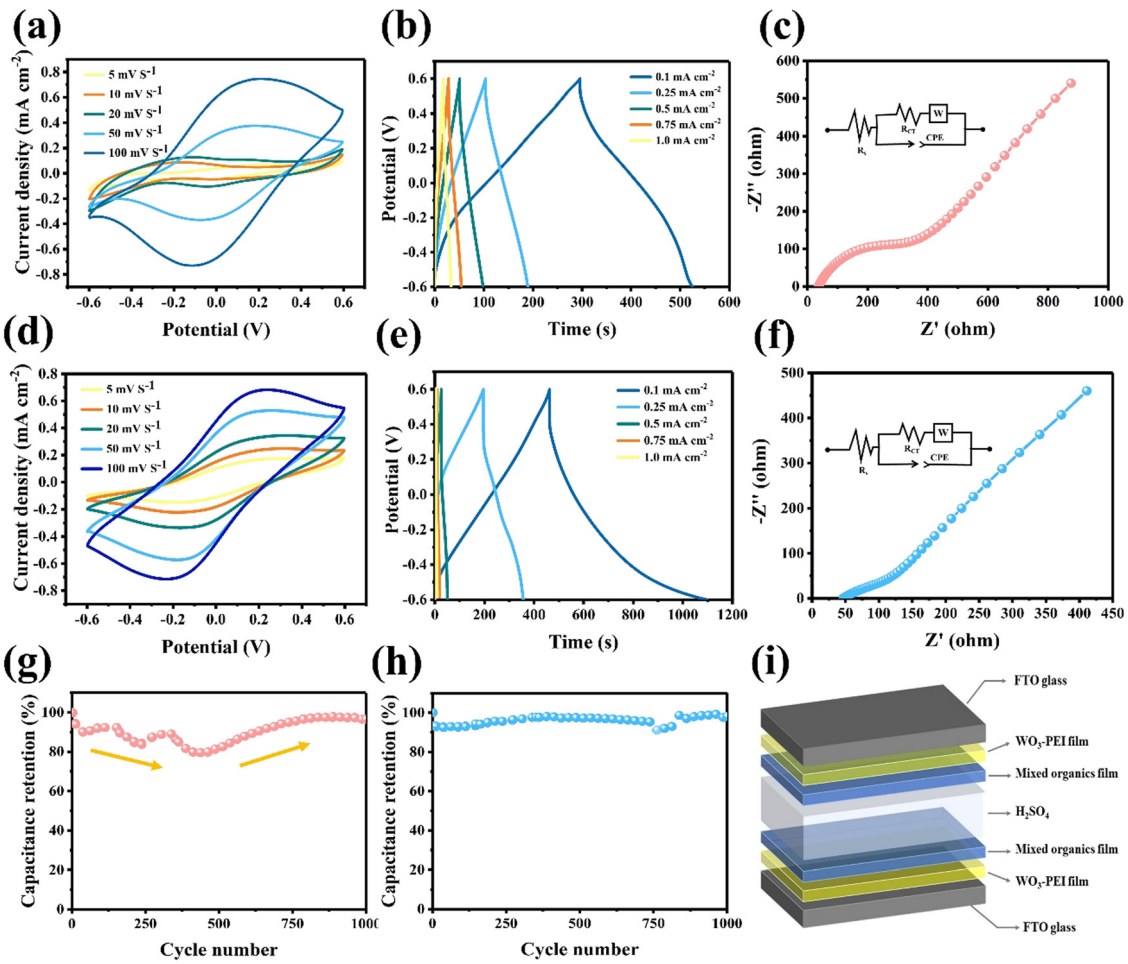

Fig. 6 (a) CV curves, (b) GCD curves, (c) EIS curve and (g) the capacitance retention rate of the WP device. (d) CV curves, (e) GCD curves, (f) EIS curve and (h) the capacitance retention rate of the WPSH device. (i) Schematic of the WPSH device.

the cycle process can be regarded as an activation process, which transforms some inactive sites into active sites and improves the original energy storage level of the material. Fig. S11d (ESI†) shows the cycle retention rate of the PSH device, which does not change much during 1000 cycles. It can also be seen that the film prepared using the organic mixture is repairable, and the device has a stable capacitance retention rate when the ions are repeatedly embedded and removed. The addition of the mixed organic film improves the capacitance retention of the WPSH device. At the end of 1000 cycles, the capacitance retention is still 98.2%. We compare the WPSH device with other similar devices in Table S3 (ESI†).[7,39,42–47]

When the redox reaction occurs with charge transfer, WO_3 and PEDOT:PSS, which are both cathodic electrochromic materials, will undergo color changes in the reduced state, so they will undergo an electrochromic process at the same time. The WP film alone is pale yellow and turns blue after charging. The individual PSH film is blue and becomes dark blue after charging. Combining the two, there is a synergistic color change. The charge and discharge of the device made of the corresponding film is related to the reversible color change. Fig. 7a–d shows the UV-VIS-NIR absorption/transmission spectra of the two coatings (WP film and WPSH film). The overall discoloration mechanism of the device is shown in Fig. 7e. When a positive voltage is applied to one of the electrodes during coloring, electrons and H^+ are de-embedded from this electrode. At the same time, $WO_3{\cdot}H_2O$ and PEDOT:PSS at the other pole are colored under negative bias by obtaining electrons to be reduced, coupled with the embedding of H^+. In contrast, both are oxidized to the initial state during the fading process.

The related pseudo-capacitive and electrochromic behaviors are derived from the redox reactions of $WO_3{\cdot}H_2O$ and PEDOT:PSS, accompanied by the insertion/extraction of H^+, as described in eqn (2) and (3):

$$WO_3{\cdot}H_2O + \alpha H^+ + \alpha e^- \Leftrightarrow H_\alpha WO_3{\cdot}H_2O \quad (2)$$

H^+ is implanted into the internal defects of the $WO_3{\cdot}H_2O$ lattice, resulting in a change in the valence state of W and a change in color.

$$PEDOT{:}PSS{:}SO_4 + 4\alpha e^- + 2\alpha H^+ \Leftrightarrow H_\alpha PEDOT{:}PSS + \alpha SO_4^{2-} \quad (3)$$

When the electric field is applied, the doping and dedoping of electrolyte ions occur between the polymer skeletons, and the energy band gap of the material changes accordingly, thereby showing the effect of discoloration.[48] In Fig. S15 (ESI†), we tested the transmission and absorption of the WPSH device and film at different voltages. In Fig. S16 and S17 (ESI†), we also tested the coloring and fading times of the WPSH device and film. The color change cycle was tested at ±2 V, and the results of the color change cycle also reflected the good self-repair performance of the modified PEDOT:PSS film.

4. Conclusion

In summary, hybrid organic films were developed by modifying PEDOT:PSS with the addition of PEG and PA. The resulting modified PEDOT:PSS hybrid organic film is capable of achieving instantaneous self-healing function following various external cuts (with an average self-healing time of 1.44 s). When the

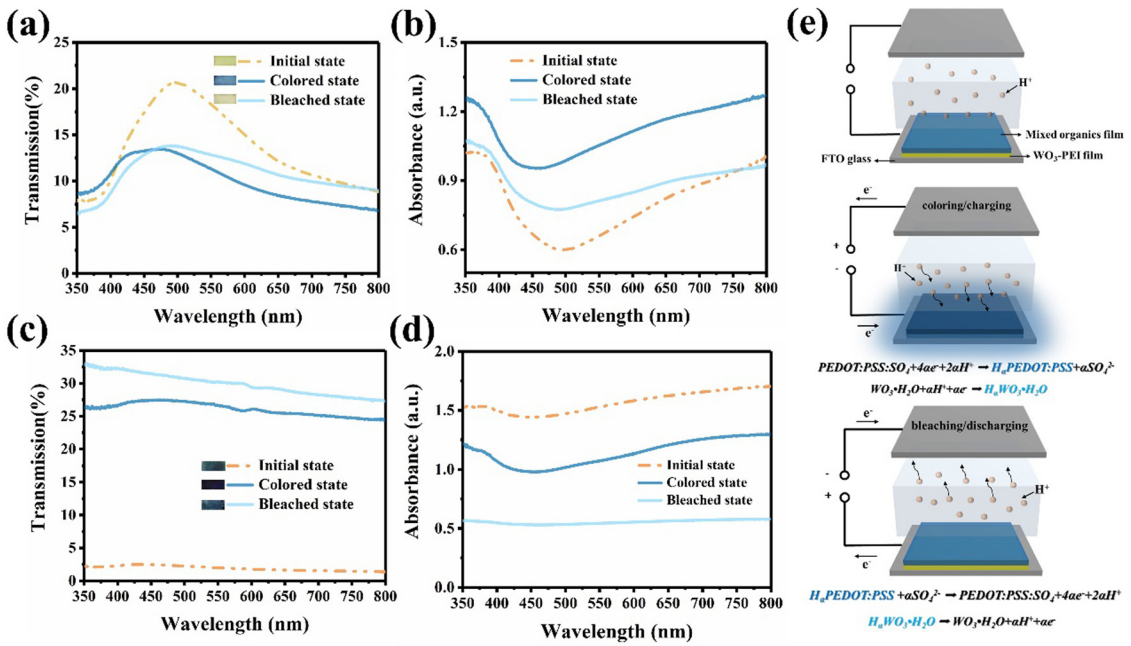

Fig. 7 (a) and (c) UV-VIS-NIR transmission spectra and (b) and (d) absorption spectra of WP films and WPSH films in the initial state, coloring state and fading state. The illustrations from top to bottom are the images of the initial state, coloring state and fading state. (e) The mechanism diagram of the WPSH film in the process of coloring/charging and fading/discharging.

film was pressed at different rates, the self-healing time was less than 0.12 s, and the retention rate reached 74% after pressing 1750 times consecutively at a rate of 8.6 cm s^{-1}. The modified PEDOT:PSS hybrid organic film was further combined with WO_3 to form a hybrid system that served as a protective layer for the WO_3 layer and exhibited synergistic color-changing behavior, thereby effectively enhancing the overall performance of the device. An EESD, which was prepared utilizing the WPSH film, showcased a retention rate of 98.2% in terms of capacitance even after being subjected to 1000 cycles at a current density of 0.5 mA cm^{-2}. At a current density of 0.1 mA cm^{-2}, a surface capacitance of 105.35 mF cm^{-2} was achieved, which was higher than the surface capacitance of 38 mF cm^{-2} of the WP device and 46 mF cm^{-2} of the PSH device, respectively. The modified PEDOT:PSS hybrid film, with its impressive self-healing capability, can be easily applied to a variety of real-world scenarios. This self-healing solution has the potential to facilitate the development of self-healing electrochemical energy storage systems and lay the foundation for the fabrication of portable electrochromic devices.

Conflicts of interest

The authors declare that they have no known competing financial interests or personal relationships that could have appeared to influence the work reported in this paper.

Acknowledgements

This work was supported by the National Natural Science Foundation of China (Grant No. 62004015 and 62004014) and the Department of Science and Technology of Jilin Province (Grant No. 20220101235JC, 20210101077JC and YDZJ202201ZYTS361).

References

1 L. Zhang, Z. Liu, X. Wu, Q. Guan, S. Chen, L. Sun, Y. Guo, S. Wang, J. Song, E. M. Jeffries, C. He, F. L. Qing, X. Bao and Z. You, *Adv. Mater.*, 2019, **31**, 1901402.
2 L. Y. Wang, L. Yuan, X. Wu, J. Wu, C. Hou and S. Feng, *RSC Adv.*, 2014, **4**, 47670–47676.
3 J. Li, J. Cao, X. Li, J. Hu, Y. Zhang, H. M. K. Sari, C. Lv, I. V. Zatovsky and W. Han, *J. Energy Chem.*, 2021, **55**, 420–427.
4 S. R. White, N. R. Sottos, P. H. Geubelle, J. S. Moore, M. R. Kessler and S. R. Sriram, *Nature*, 2001, **409**, 794–797.
5 W. Du, Y. Jin, S. Lai, L. Shi, W. Fan and J. Pan, *Polymer*, 2018, **158**, 120–129.
6 R. Zheng, J. Zhang, C. Jia, Z. Wan, Y. Fan, X. Weng, J. Xie and L. Deng, *Polym. Chem.*, 2017, **8**, 6981–6988.
7 R. Zheng, Y. Fan, Y. Wang, Z. Wan, C. Jia, X. Weng, J. Xie and L. Deng, *Electrochim. Acta.*, 2018, **286**, 296–303.
8 J.-N. Liu, Q. He, M.-Y. Pan, K. Du, C.-B. Gong and Q. Tang, *J. Mater. Chem. A*, 2022, **10**, 25118–25128.
9 Y. Zhao, Y. Zhang, H. Sun, X. Dong, J. Cao, L. Wang, Y. Xu, J. Ren, Y. Hwang, I. H. Son, X. Huang, Y. Wang and H. Peng, *Angew. Chem., Int. Ed.*, 2016, **55**, 14384–14388.
10 J. Liu, J. Long, Z. Shen, X. Jin, T. Han, T. Si and H. Zhang, *Adv. Sci.*, 2021, **8**, 2004689.
11 X. Li, D. Lou, H. Wang, X. Sun, J. Li and Y. Liu, *Adv. Funct. Mater.*, 2020, **30**, 2007291.
12 N. Chodankar, S. Patil, S. Hwang, S. Karekar, K. Jayaramulu, W. Zhang, D. Dubal, Y. Huh and Y. Han, *J. Mater. Chem. A.*, 2021, **9**, 26603–26627.
13 J. P. Thomas, L. Zhao, D. Mcgillivray and K. T. Leung, *J. Mater. Chem. A*, 2014, **2**, 2383–2389.
14 L. V. KayserD and J. Lipomi, *Adv. Mater.*, 2019, **31**, 1806133.
15 Y. Li, X. Li, S. Zhang, L. Liu, N. Hamad, S. R. Bobbara, D. Pasini and F. Cicoira, *Adv. Funct. Mater.*, 2020, **30**, 2002853.
16 S. Zhang and F. Cicoira, *Adv. Mater.*, 2017, **29**, 1703098.
17 J. Y. Oh, S. Kim, H. K. Baik and U. Jeong, *Adv. Mater.*, 2016, **28**, 4455–4461.
18 Y. Li, S. Zhang, X. Li, V. R. N. Unnava and F. Cicoira, *Flex. Print. Electron.*, 2019, **4**, 044004.
19 S. Vogel and R. Holze, *Electrochim. Acta.*, 2005, **50**, 1587–1595.
20 D. T. Gillaspie, R. C. Tenent and A. C. Dillon, *J. Mater. Chem.*, 2010, **20**, 9585–9592.
21 H. Ling, J. Lu, S. Phua, H. Liu, L. Liu, Y. Huang, D. Mandler, P. S. Lee and X. Lu, *J. Mater. Chem. A*, 2014, **2**, 2708–2717.
22 G. Gunbas and L. Toppare, *Chem. Commun.*, 2012, **48**, 1083–1101.
23 Z. Yang, J. Ma, B. Bai, A. Qiu, D. Losic, D. Shi and M. Chen, *Electrochim. Acta.*, 2019, **322**, 134769.
24 Z. Bi, X. Li, X. He, Y. Chen, X. Xu and X. Gao, *Sol. Energy Mater. Sol. Cells*, 2018, **183**, 59–65.
25 C. Costa, C. Pinheiro, I. Henriques and C. A. Laia, *ACS Appl. Mater. Interfaces*, 2012, **4**, 1330–1340.
26 H. Zhang, H. Zhao, Y.-Q. Jiang, S.-Y. Hou, Z.-H. Zhou and H.-L. Wan, *Inorganica Chim. Acta.*, 2003, **351**, 311–318.
27 D. Zhou, F. Shi, D. Xie, D. H. Wang, X. H. Xia, X. L. Wang, C. D. Gu and J. P. Tu, *J. Colloid Interface Sci.*, 2016, **465**, 112–120.
28 Z. Wang, P. Tammela, J. Huo, P. Zhang, M. Strømme and L. Nyholm, *J. Mater. Chem. A*, 2016, **4**, 1714–1722.
29 S. Khan, M. Ul-Islam, W. A. Khattak, M. W. Ullah and J. K. Park, *Carbohydr. Polym.*, 2015, **127**, 86–93.
30 M. Lay, M. A. Pelach, N. Pellicer, J. A. Tarres, K. N. Bun and F. Vilaseca, *Carbohydr. Polym.*, 2017, **165**, 86–95.
31 B. Yang, P. R. F. Barnes, Y. Zhang and V. Luca, *Catal. Lett.*, 2007, **118**, 280–284.
32 C.-Y. Kim, M. Lee, S.-H. Huh and E.-K. Kim, *J. Solgel Sci. Technol.*, 2009, **53**, 176–183.
33 M. Breedon, P. Spizzirri, M. Taylor, J. Du Plessis, D. Mcculloch, J. Zhu, L. Yu, Z. Hu, C. Rix, W. Wlodarski and K. Kalantar-Zadeh, *Cryst. Growth Des.*, 2009, **10**, 430–439.
34 S. E. Mcelwain, T. A. Blanchet, L. S. Schadler and W. G. Sawyer, *Tribol. Trans.*, 2008, **51**, 247–253.
35 D. L. BurrisW and G. Sawyer, *Tribol. Trans.*, 2005, **48**, 147–153.

36 X. Peng, W. Wang, W. Yang, J. Chen, Q. Peng, T. Wang, D. Yang, J. Wang, H. Zhang and H. Zeng, *J. Colloid Interface Sci.*, 2022, **618**, 111–120.
37 Q. Li, L. Cao, W. Wang, X. Qin and S. Chen, *Composites, Part A*, 2022, **163**, 107213.
38 S. Wang and M. W. Urban, *Nat. Rev. Mater.*, 2020, **5**, 562–583.
39 J. R. Yin, J. L. Li, L. Y. Wang, B. Cai, X. Yang, X. Li and W. Lü, *J. Energy Storage*, 2022, **51**, 104460.
40 Y. Meng, J. Yin, L. Wang, X. Yang, X. Li and Y. Jiang, *Mater. Lett.*, 2023, **335**, 133809.
41 X. Huo, R. Li, J. Wang, M. Zhang and M. Guo, *Chem. Eng. J.*, 2022, **430**, 132821.
42 K.-W. Kim, T. Y. Yun, S.-H. You, X. Tang, J. Lee, Y. Seo, Y.-T. Kim, S. H. Kim, H. C. Moon and J. K. Kim, *NPG Asia Mater.*, 2020, **12**, 84.
43 S. Y. Kim, T. Y. Yun, K. S. Yu and H. C. Moon, Reliable, *ACS Appl. Mater. Interfaces*, 2020, **12**, 51978–51986.
44 M. Zhu, Y. Huang, Y. Huang, W. Meng, Q. Gong, G. Li and C. Zhi, *J. Mater. Chem. A*, 2015, **3**, 21321–21327.
45 Z. Bi, X. Li, Y. Chen, X. He, X. Xu and X. Gao, *ACS Appl. Mater. Interfaces*, 2017, **9**, 29872–29880.
46 S. Wang, H. Xu, T. Hao, M. Xu, J. Xue, J. Zhao and Y. Li, *Appl. Surf. Sci.*, 2022, **577**, 151889.
47 Y. Wang, R. Zheng, J. Luo, H. A. Malik, Z. Wan, C. Jia, X. Weng, J. Xie, L. Deng and X. Yao, *Electrochim. Acta.*, 2019, **320**, 134489.
48 S. Kee, H. Kim, S. H. K. Paleti, A. El Labban, M. Neophytou, A.-H. Emwas, H. N. Alshareef and D. Baran, *Chem. Mater.*, 2019, **31**, 3519–3526.

